CORROSION BEHAVIOR OF DIFFERENT MATERIALS IN CORROSIVE MEDIA OF CHEMICAL EQUIPMENT

Longfei ZHU[1], Guandong WANG[2], Yang WANG[3*], Wei CUI[4], Chuntao SHI[5]

In order to comprehensively investigate the corrosion behavior of four distinct materials, namely S30408, S31603, C-276, and TA2, subjected to various chloride-rich corrosive media within a petrochemical facility, laboratory simulations of full immersion tests were conducted utilizing three distinct chloride corrosion solutions sourced directly from the field. Scanning electron microscopy (SEM) was employed to scrutinize the microstructural characteristics of the materials. Based on the corrosion phenomena observed in the field, specifically hydrochloric acid-induced corrosion, HCl solutions with varying chloride ion concentrations of 5%, 10%, and 20% were prepared to simulate corrosive environments with different chloride concentrations. Electrochemical investigations, encompassing open circuit potential measurements, tafel curve analysis, and AC impedance conducted on the materials S30408, S31603, C-276, and TA2. The experimental results reveal that the corrosion rates of the four materials, as assessed in the full immersion tests, are ranked from lowest to highest as follows: TA2, C-276, S31603, and S30408. Through electrochemical testing, combining Tafel curve, self-corrosion current density, and the impedance values from electrochemical impedance spectroscopy, the corrosion resistance of the materials, ranked from strongest to weakest, is as follows: TA2, C-276, S31603, and S30408.

Keywords: Cl- corrosion; Total immersion experiments; SEM; Electrochemical tests; Corrosion resistance

1. Introduction

With the continuous advancement of both scientific technology and global economies, the demand for epoxy resins, both domestically and internationally, has been steadily rising. During the production of epoxy resin raw materials, the rapid cooling tower and heat exchanger serve as crucial heat exchange equipment, requiring prolonged operation in complex and harsh environments. These systems are frequently subjected to high temperatures, elevated pressures, and corrosive media, where prolonged operation can result in material degradation.

[1] School of Intelligent Manufacturing Modern Industry, Xinjiang University, Xinjiang, China
[2] Sinopec Hunan Petrochemical Co, Hunan, China
[3] School of Intelligent Manufacturing Modern Industry, Xinjiang University, Xinjiang, China, corresponding author, e-mail address: wy830052@126.com
[4] China Special Equipment Inspection and Research Institute, Beijing, China
[5] China Special Equipment Inspection and Research Institute, Beijing, China

Consequently, reasonable selection of materials is critical to the dependability and stable operation of the equipment. In industrial applications, corrosion resistance is a critical factor for ensuring the safe utilization of materials [1]. S30408 stainless steel, S31603 stainless steel, Hastelloy C-276, and TA2 titanium alloy are widely utilized engineering materials, each exhibiting distinct mechanical properties and corrosion resistance, making them prevalent in chemical equipment. S31603 stainless steel is an upgraded variant of S30408 stainless steel, enriched with molybdenum, which significantly enhances its corrosion resistance. As a result, S31603 stainless steel finds extensive application in various engineering sectors [2-4]. Hastelloy C-276 stands as one of the most corrosion-resistant materials in modern metallurgy, offering exceptional resistance to a broad spectrum of corrosive media. Consequently, it is particularly suited for use in highly corrosive environments, such as the petrochemical industry and other demanding sectors. In contrast, TA2 titanium alloy is renowned for its lightweight, high strength, exceptional high-temperature resistance, and superior corrosion resistance. Titanium and its alloys exhibit remarkable resistance to acidic, alkaline, and saline corrosion, rendering them ideal for applications in offshore, aerospace, and chemical industries. Specifically, the superior corrosion resistance of TA2 makes it a promising material for applications such as piping, evaporators [5], aerospace and medical devices [6], and marine facilities [7,8]. Although these materials demonstrate varying degrees of corrosion resistance across diverse conditions, discrepancies in their performance under specific environmental factors, such as those found in rapid cooling towers and heat exchangers, necessitate further experimental investigation. This study experimentally verifies the corrosion behavior of these four materials in typical corrosive media encountered in emergency cooling towers and heat exchangers, with the objective of providing a theoretical foundation for material selection in engineering practice. By comparing the corrosion behaviors of different materials in simulated operational environments, a more comprehensive understanding of material performance in real-world applications can be attained, thereby guiding the long-term operation of chemical equipment.

2. Experimental

2.1 Total immersion experiment

This study investigates the corrosion behavior of materials in an organochlorine device, focusing on chloride-induced corrosion. In the laboratory, a full immersion experiment was conducted under three distinct conditions to simulate real-world corrosive environments. The specimens consisted of four materials: S30408, S31603, C-276, and TA2. The chemical composition of each material is shown in Table 1, and the standard used is GB/T 20878-2020.The

specimens were processed into dimensions of 45 mm × 15 mm × 3 mm and 20 mm × 20 mm × 3 mm. The corrosion rate of the larger specimens was determined using the loss-in-weight method, while the smaller specimens were characterized using a ZEISS EVO10 scanning electron microscope. The corrosion morphology of the four materials was compared under identical temperature conditions in different organic chloride corrosion media. The three corrosive media used in the experiments were solutions collected from a petrochemical organochlorine plant operating under real-world conditions. Solution 1 comprised propylene, chloride, and hydrogen chloride, solution 2 contained crude chloropropene, and solution 3 was composed of monochloropropanol. The experimental temperature 60°C to replicate the working conditions in the field, and the duration of the experiment was 7 days. Initially, the specimens were cleaned and degreased using propanol, followed by ultrasonic cleaning and drying with cold air. The specimens were then weighed, and the initial weight was recorded. At the conclusion of the experiment, the specimens were acid-washed, re-weighed, and the corrosion rate was calculated using the weight loss method. The corrosion rate was then determined using the following formula:

$$R = \frac{3650 \times (W1 - W2)}{STρ} \quad (1)$$

Where: R represents the corrosion rate (mm/year); W_1 is the weight of the specimen before corrosion (g); W_2 is the weight after corrosion (g); S denotes the total surface area of the specimen (cm^2); T is the experimental duration (days); ρ is the specimen density (g/cm^3). The experiments were conducted using a high-temperature, high-pressure reactor for the immersion tests, which were designed to simulate real operational conditions. According to the different annual corrosion rate of the metal can be corrosion resistance according to the Chinese Society of Corrosion and Protection edited by (metal protection manual) will be divided into 10 levels of corrosion resistance of metal materials, as shown in Table 2.

Table 1

Major elemental compositions of the four materials (mass fractions) %

Material	C	Si	Mn	S	Ni	Cr	Mo	Fe	Ti
S30408	0.054	0.41	1.2	0.003	8.15	18.3	-	71.843	-
Standard	≤0.08	≤1.00	≤2.00	≤0.03	8.0~10.5	18.0-20.0	-	Bal.	-
S31603	0.016	0.51	1.13	0.008	10.72	16.88	2.13	68.575	-
Standard	≤0.03	≤1.00	≤2.00	≤0.03	10.0~14.0	16.0~18.0	2.0~3.0	Bal.	-
Material	C	Si	Mn	W	Ni	Cr	Mo	Fe	Ti
C-276	0.005	-	0.412	3.21	60.641	16.115	13.882	5.736	-
Standard	≤0.01	-	≤1.00	3.0~4.5	≥57	14.5~16.5	15.0~17.0	4.0~7.0	-
TA2	0.02	0.04	-	-	-	-	-	0.18	99.94
Standard	≤0.03	≤0.1	-	-	-	-	-	≤0.30	≥99.2

Table 2

Corrosion resistance grade classification

Corrosion resistance classification	Corrosion resistance grade	Corrosion rate (mm/year)
Fully corrosion resistant	Level 1	< 0.001
Very corrosion resistant	Level 2	0.001~0.005
Very corrosion resistant	Level 3	0.005~0.01
Corrosion resistant	Level 4	0.01~0.05
Corrosion resistant	Level 5	0.05~0.1
Moderate corrosion resistant	Level 6	0.1~0.5
Moderate corrosion resistant	Level 7	0.5~1.0
Lack of corrosion resistance	Level 8	1.0~5.0
Lack of corrosion resistance	Level 9	5.0~10.0
Not resistant to corrosion	Level 10	> 10.0

2.2 Electrochemical testing

The specimens were prepared with dimensions of 10 mm × 10 mm × 3 mm for electrochemical testing. The connecting wires were sealed with cold-setting epoxy resin, and the working surface, with an area of 1 cm^2, was progressively sanded using sandpaper and polished. Finally, the specimens were degreased, cleaned, and dried using anhydrous ethanol. Electrochemical testing of the four material specimens was conducted using a Chenhua CHI660E electrochemical workstation. The experiments were carried out at an experimental temperature of 60°C, with the cooling tower and two heat exchangers exposed to media containing chloropropylene, propylene, propanol, and elevated concentrations of hydrochloric acid, which served as the primary source of corrosive agents. Chloropropene, propylene, and propanol are non-electrolyte solutions, meaning that metals immersed in these media will not undergo electron loss in chemical reactions. The primary corrosion factor in this study is hydrochloric acid. Therefore, electrochemical tests were conducted using simulated corrosion solutions with varying mass fractions of hydrochloric acid (5%, 10%, and 20%). A conventional three-electrode system was employed, Reference electrode: silver/silver chloride (Ag/AgCl), auxiliary electrode: platinum sheet, working electrode: the four materials under investigation. Prior to testing, the samples were immersed in the test solution for 600 seconds to measure the open circuit potential.The system was stabilized before experimentation to ensure that potential fluctuations remained within ±5 mV.Electrochemical impedance spectroscopy (EIS) was performed using the open circuit potential as input, with a 5 mV amplitude and a frequency range of 10^5-10^{-2} Hz.For Tafel curve analysis, a scan rate of 1 mV/s was employed, with a potential range of ±0.5 V from the OCP.

3. Results and Discussion

3.1 Corrosion behavior of four materials in different chloride corrosive media at 60°C

3.1.1 Corrosion rate analysis

As shown in Fig. 1, after seven days of full immersion simulation at 60°C in a propylene/chloride/hydrogen chloride corrosive medium, the corrosion rates for TA2, C-276, S31603, and S30408 were 0.0079 mm/year, 0.0258 mm/year, 0.0599 mm/year, and 0.1240 mm/year, respectively. According to the metal corrosion manual, which classifies the corrosion resistance of metal materials into ten levels, the corrosion resistance of the four materials is as follows: TA2 exhibited corrosion resistance at level 3 (0.005–0.01 mm/year, very corrosion-resistant), C-276 at level 4 (0.01–0.05 mm/year, very corrosion-resistant), S31603 at level 5 (0.05–0.1 mm/year, corrosion-resistant), and S30408 at level 6 (0.1–0.5 mm/year, moderately corrosion-resistant). Among these, TA2 displayed the highest corrosion resistance, followed by C-276 and 316L in decreasing order, with 304 showing the lowest corrosion resistance.

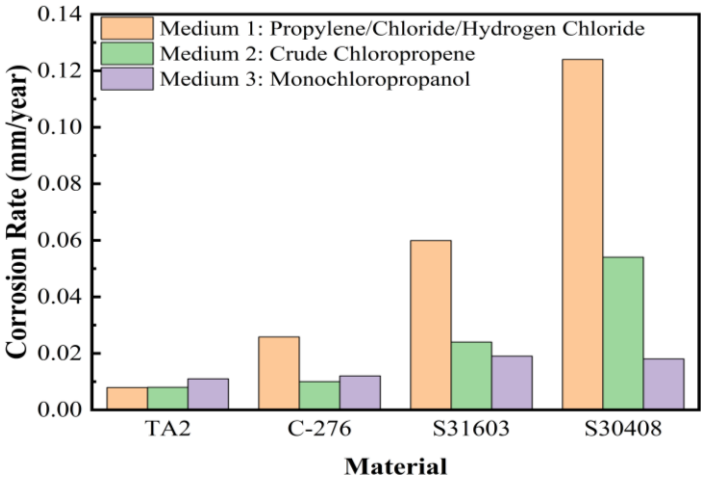

Fig.1 Corrosion rates of four materials in different organochloride corrosive media

In a crude chloropropene medium at 60°C, the corrosion rates for TA2, C-276, S31603, and S30408 were 0.008 mm/year, 0.01 mm/year, 0.024 mm/year, and 0.054 mm/year, respectively. The corrosion resistance of the four materials is as follows: TA2 exhibited corrosion resistance grade 3 (0.005–0.01 mm/year, very resistant), C-276 and S31603 both exhibited corrosion resistance grade 4 (0.01–0.05 mm/year, very resistant), and S30408 exhibited corrosion resistance grade 5 (0.05–0.1 mm/year, corrosion-resistant). C-276 and S31603 both exhibited corrosion resistance grade 4 (0.01–0.05 mm/year, very corrosion resistant), while

S30408 exhibited corrosion resistance grade 5 (0.05–0.1 mm/year, corrosion resistant). Among these materials, TA2 demonstrated the highest corrosion resistance, followed by C-276 and S31603 in descending order, with S30408 exhibiting the lowest resistance to corrosion.

In a monochloropropanol corrosive medium at 60°C, the corrosion rates for TA2, C-276, S31603, and S30408 were 0.011 mm/year, 0.012 mm/year, 0.019 mm/year, and 0.018 mm/year, respectively. The corrosion resistance of all four materials was classified as grade 4 (0.01–0.05 mm/year, very corrosion resistant). All four materials showed significant corrosion resistance in monochloropropanol solution.

3.1.2 Surface morphology analysis

Fig. 2 illustrates the SEM images of four materials in various solutions, showcasing their surface morphology.

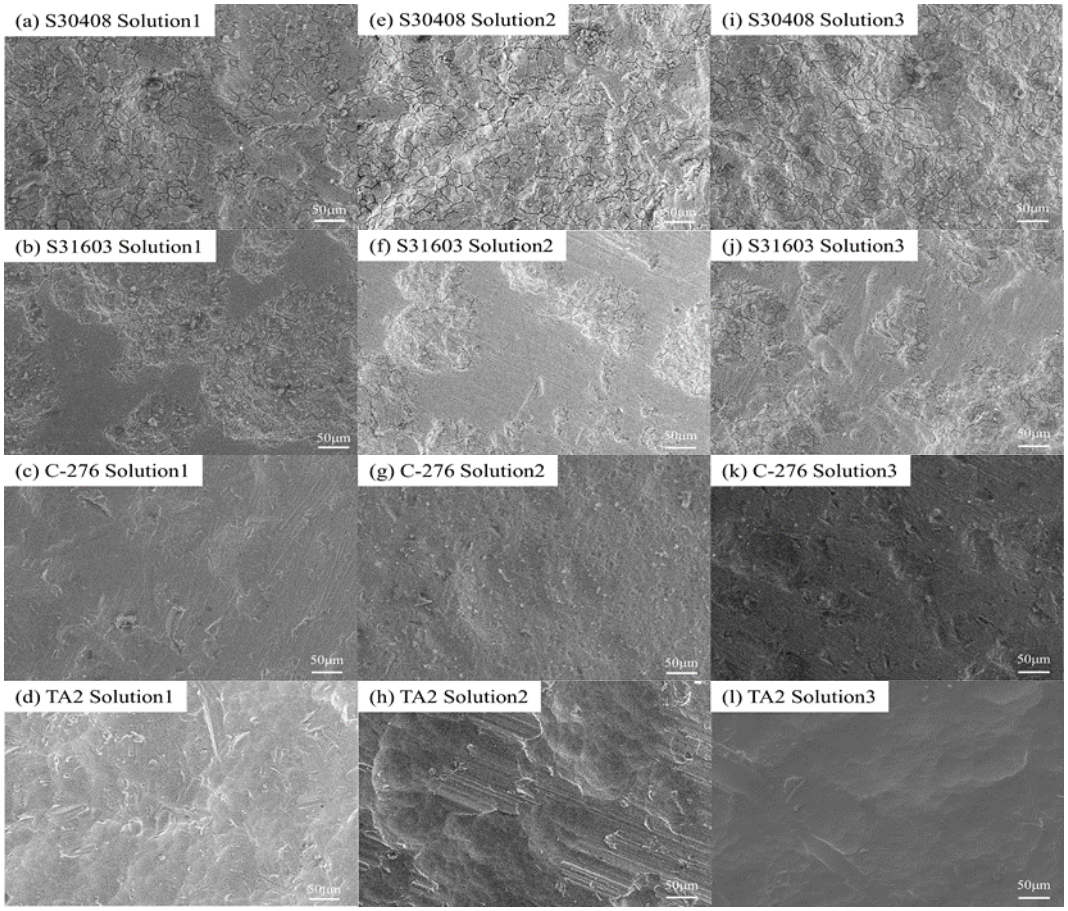

Fig. 2 SEM images of four materials in different organochloride corrosive media

As observed in Figs. 2(a), 2(e), and 2(i), the surface of S30408 stainless steel in various organic chloride corrosive media exhibited distinct grain-boundary-preferential corrosion, with the corrosion morphology extending along the grain boundaries. S30408 stainless steels show surface corrosion with preferential growth of morphology along the grain boundaries; the grain interiors remain basically intact, showing typical intergranular corrosion characteristics.Although the materials have low carbon content and did not experience sensitization heat exposure, traditional carbide precipitation-type intergranular corrosion is not likely to occur.However, in the strong Cl^- and HCl environment, the grain boundary passivation film is more prone to local failure, induced by interfacial electrochemical inhomogeneity, which triggers the selective dissolution of grain boundaries.

Fig. 2(b), Fig.2(f), and Fig.2(j) show that S31603 stainless steel also exhibits a pronounced tendency to corrode at grain boundaries in various organic chloride corrosive media. However, compared to S30408 stainless steel, the degree of corrosion is less severe, and the corrosion marks are mainly confined to the grain boundaries. This suggests that despite its better corrosion resistance than S30408, S31603 is still susceptible to the influence of Cl^- ions, leading to intergranular corrosion [9,10]. Despite the good mechanical properties of conventional S30408 and S31603 austenitic stainless steels [11], they are susceptible to intergranular corrosion due to the strong Cl^- corrosive environment in this study. This can significantly reduce material strength and pose a serious hazard to the production process. Their strength may not fully meet the required application criteria due to the occurrence of intergranular corrosion [12,13].

The surface morphology of the C-276 alloy, as shown in Figs. 2(c), 2(g), and 2(k), appears relatively smooth in each corrosive medium, with no visible corrosion traces or corrosion products. This behavior is attributed to the high molybdenum and chromium content in C-276, which effectively resists Cl-erosion. Additionally, the inclusion of tungsten further enhances its overall corrosion resistance. Fig.s 2(d), 2(h), and 2(l) illustrate the surface morphology of TA2 titanium alloy, revealing the absence of visible corrosion products or traces in various organic chloride corrosive media, thus confirming its robust corrosion resistance. In summary, the SEM images clearly show that 304 stainless steel exhibits the most severe corrosion, followed by 316L stainless steel. In contrast, both C-276 and TA2 display exceptional corrosion resistance under identical corrosive conditions, with no discernible corrosion signs on their surfaces.

3.2 Electrochemical testing

3.2.1 Tafel curve analysis

Fig. 3(a) illustrates the Tafel polarization curves for four materials—S30408, S31603, C-276, and TA2—at 60°C with a 5% HCl concentration. The

Tafel extrapolation method enables the determination of the corrosion potential (E_{corr}) and corrosion current density (i_{corr}) for the four materials from the Tafel intercepts. The Ecorr and icorr, obtained in accordance with ASTM G59-97(2020), offer valuable insights into the susceptibility of these materials to corrosion onset. A more electropositive corrosion potential suggests that the material exhibits enhanced resistance to anodic polarization. The corrosion current density serves as an indicator of the metal's dissolution rate during the corrosion process. A higher corrosion current density correlates with an increased dissolution rate of the metal [14,15]. As depicted in Fig. 3(a) and Table 3, at 60°C with a 5% HCl concentration, the corrosion potentials of the four materials vary significantly, arranged from negative to positive as follows: S30408, S31603, C-276, and TA2. The corrosion current densities of the four materials, ranked from highest to lowest, are as follows: S30408, S31603, C-276, and TA2. As shown in Fig. 3(b) and Table 3, at 60°C with a 10% HCl concentration, the corrosion potentials of the four materials differ markedly, arranged from negative to positive in the following order: S30408, S31603, C-276, and TA2. The corrosion current densities for the four materials, in descending order, are as follows: S30408, S31603, C-276, and TA2. As illustrated in Fig. 3(c) and Table 3, at 60°C with a 20% HCl concentration, the corrosion potentials of the four materials differ substantially, in the following order from negative to positive: TA2, S30408, S31603, and C-276. The corrosion current densities for the four materials, ranked from highest to lowest, are as follows: S30408, S31603, TA2, and C-276.

As illustrated in Fig. 3(a), S31603 demonstrates a modest peak in the anodic branch at a 5% HCl concentration, which can be attributed to the adsorption of impurities from the solution, leading to a modification of the solution-metal interface structure. In the anodic branch, it is evident that all three of the other materials undergo passivation, leading to the film on the specimen surface, thereby inhibiting corrosion. Fig.s 3(b) and 3(c) reveal that, across varying concentrations of hydrochloric acid solutions, the anodic branches of all four materials undergo passivation. As presented in Table 3, TA2 displays a more negative corrosion potential at a 20% HCl concentration when compared to the other three materials. However, its corrosion current density is lower, as the corrosion potential represents a thermodynamic parameter that reflects the propensity for corrosion reactions to occur [16,17]. although it does not directly correlate with the corrosion rate. As presented in Table 3, the corrosion current densities of S30408, S31603, and TA2 increase with the increase in hydrochloric acid concentration, suggesting that the elevated chloride ion content in higher acid concentrations significantly influences the corrosion current densities of these materials. In contrast, the corrosion current density of C-276 decreases as the acid concentration increases, which can be attributed to the presence of elements such as chromium, molybdenum, and tungsten in the C-276 alloy, which facilitate the

formation of a stable oxide passivation film in acidic environments. The enhancement of this passivation film results in a reduction of the electrochemical reaction rate and a corresponding decrease in current density.

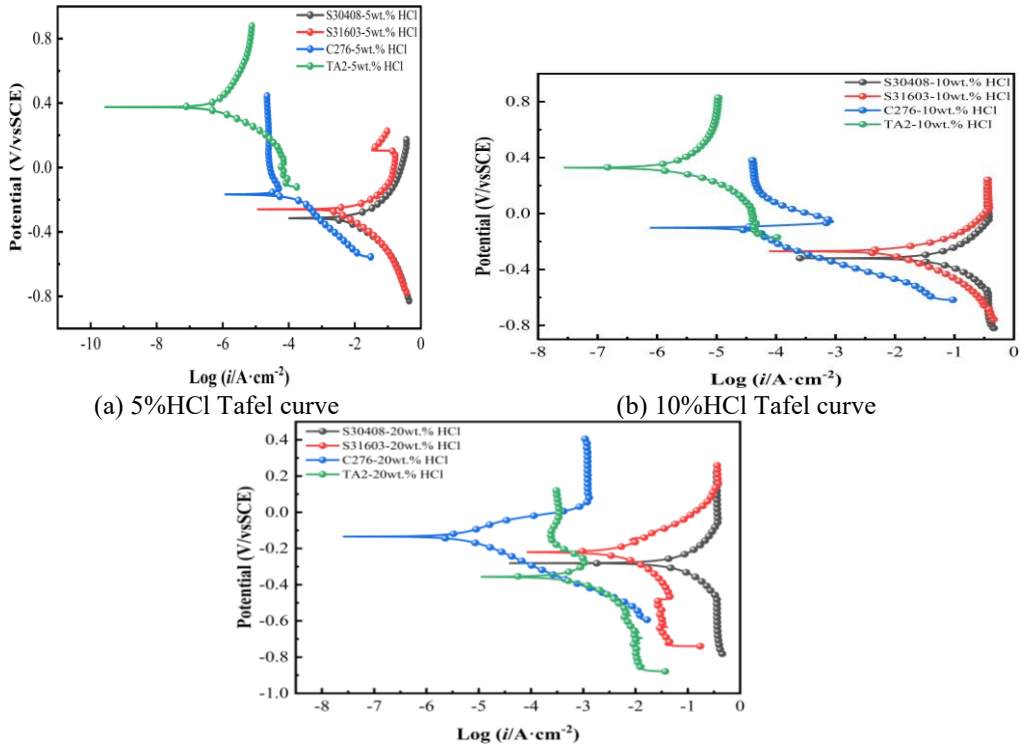

(a) 5%HCl Tafel curve (b) 10%HCl Tafel curve

(c) 20%HCl Tafel curve

Fig.3 Tafel curves of four materials under different concentrations of hydrochloric acid

Table 3

corrosion potentials and corrosion current densities of four materials under different concentrations of hydrochloric acid

Medium (HCl wt%)	Material	i_{corr} (A/cm^{-2})	E_{corr} (V)
5	S30408	1.009×10^{-2}	-0.315
5	S31603	8.502×10^{-3}	-0.260
5	C-276	2.075×10^{-4}	-0.167
5	TA2	5.834×10^{-7}	0.375
10	S30408	5.596×10^{-2}	-0.320
10	S31603	1.060×10^{-2}	-0.270
10	C-276	9.596×10^{-5}	-0.102
10	TA2	2.017×10^{-6}	0.328
20	S30408	7.968×10^{-2}	-0.281
20	S31603	5.461×10^{-2}	-0.220
20	C-276	3.857×10^{-6}	-0.134
20	TA2	1.323×10^{-3}	-0.356

3.2.2 AC impedance analysis

Fig. 4 presents the electrochemical impedance spectra of the four materials at 60°C under different concentrations of hydrochloric acid. The equivalent circuit depicted in Fig. 5 was employed for impedance fitting using Zview software, With the fitting parameters summarized in Table 4, Fig. 5(a) illustrates the equivalent circuit diagrams for S30408 and S31603, where R1: solution resistance, CP1 and R2: equivalent capacitance and charge transfer resistance of the double electric layer, L: equivalent inductance, R3: equivalent resistance. Fig. 5(b) presents the equivalent circuit diagrams of C-276 and TA2 in 5% and 10% HCl solutions, where R1: solution resistance, CP1 and R2: bilayer capacitance and charge transfer resistance, Fig. 5(c) illustrates the equivalent circuit diagrams of C-276 and TA2 in a 20% HCl solution, where R1: solution resistance, CP1 and R2: bilayer capacitance and charge transfer resistance, CP2 and R3: bilayer capacitance and charge transfer resistance of the membrane layer, The fitting results are summarized in Table 4.

Fig. 4(a), Fig. 4(c), and Fig. 4(e) present the Nyquist plots for 5%, 10%, and 20% HCl solutions, respectively, while Fig.s 4(b), 4(d), and 4(f) depict the corresponding Bode plots. As observed in Fig. 4(a), the capacitance arc radius of TA2 is larger than those of the other three materials, which indicates a higher charge transfer resistance. A larger capacitance arc radius corresponds to a higher charge transfer resistance, which in turn reflects superior corrosion resistance of the material [18]. In contrast, the capacitance arc of C-276, S30408, and S31603 gradually decreases, and the Nyquist plots of S31603 and S30408 stainless steel exhibit high-frequency capacitance circuits and low-frequency inductive circuits, with the presence of inductive circuits suggesting that some or all of the surface area remains active during corrosion [19,20]. The impedance fitting results in Table 4 reveal the following corrosion resistance ranking of the four materials: TA2 > C-276 > S31603 > S30408.

As shown in Fig. 4(c), the capacitive arc radius indicates that TA2 exhibits superior corrosion resistance compared to the other three materials. The impedance results presented in Table 4 allow for the derivation of impedance fitting parameters, which reveal the relative impedance of the four materials in the following order: S30408 < S31603 < C-276 < TA2. As illustrated in Fig. 4(e), with the increase in hydrochloric acid concentration and chlorine ion concentration, the impedance radius of C-276 demonstrates significantly better performance compared to the other three materials. This is due to the synergistic effects of molybdenum, chromium, and tungsten in the alloy, which facilitate the formation of a more compact oxide protective layer, thereby effectively preventing further corrosion.The impedance radius of TA2 in 20% HCl is notably smaller than that of C-276, This is due to the instability of the film formed on the surface of the TA2 specimen when exposed to high chloride concentrations,

which leads to film rupture and a reduced impedance radius. Chloride ion concentration exerts a significant influence on the corrosion resistance of all different materials [21].

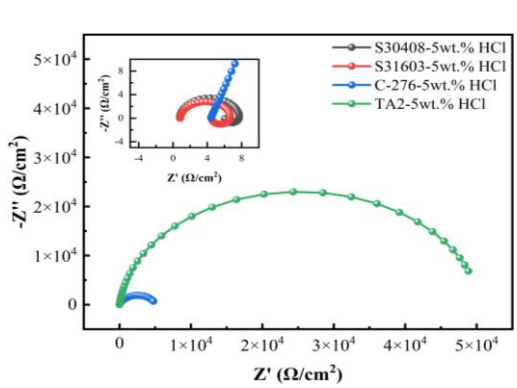

(a) 5%HCl Nyquist

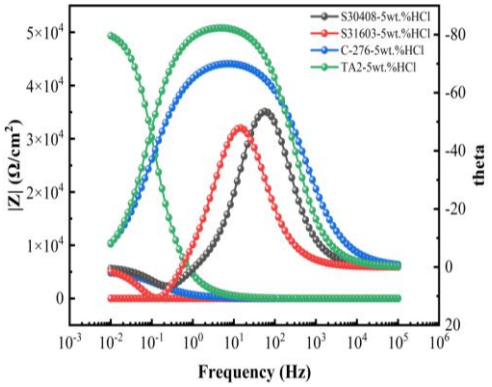

(b) 5%HCl Bode

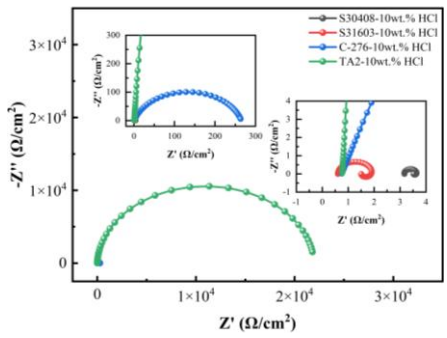

c) 10%HCl Nyquist

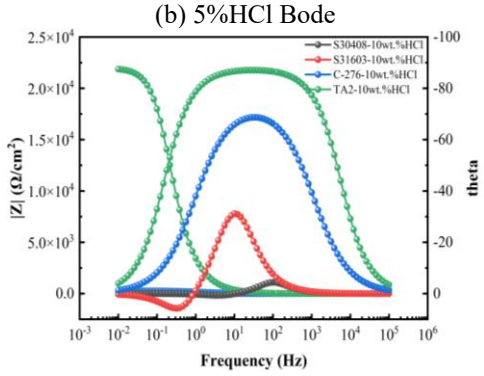

(d) 10%HCl Bode

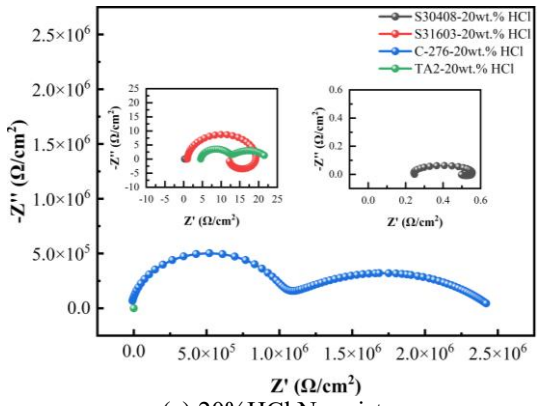

(e) 20%HCl Nyquist

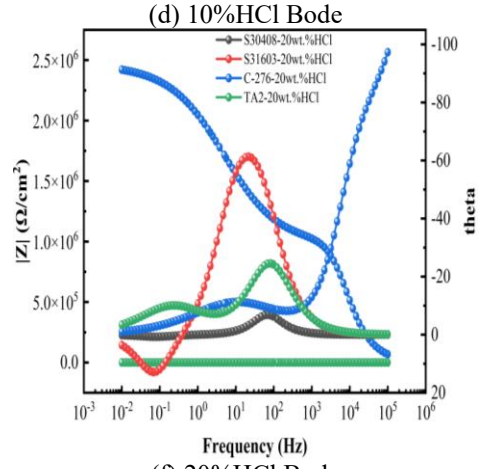

(f) 20%HCl Bode

Fig. 4 Impedance diagrams of four materials under different concentrations of hydrochloric acid

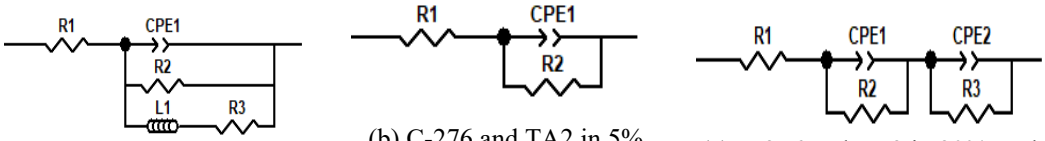

(a) S30408 and S31603 equivalent circuits

(b) C-276 and TA2 in 5% HCl and 10% HCl equivalent circuits

(c) C-276 and TA2 in 20% HCl equivalent circuits

Fig.5 Equivalent circuit diagram

Table 4

Electrochemical impedance parameters of four materials at different concentrations of hydrochloric acid

Material	Medium (wt%)	R1 (Ω/cm^2)	C1 (mF/cm^{-2})	R2 (Ω/cm^2)	C2 (mF/cm-2)	L1 (mH/cm^2)	R3 (Ω/cm^2)
S30408	5	0.796	1.351×10^{-3}	7	-	15.17	21.09
S31603	5	0.842	6.706×10^{-3}	6.024	-	13.52	9.383
C-276	5	4.415	2.950×10^{-4}	5077	-	-	-
TA2	5	22.68	3.825×10^{-5}	50444	-	-	-
S30408	10	3.171	2.382×10^{-3}	0.467	-	0.060	1.432
S31603	10	0.606	2.165×10^{-2}	1.363	-	1.333	2.647
C-276	10	0.751	8.628×10^{-4}	264..3	-	-	-
TA2	10	0.771	4.754×10^{-5}	21984	-	-	-
S30408	20	0.448	2.521×10^{-2}	0.126	-	3.258	1.587
S31603	20	0.984	2.226×10^{-3}	18.66	-	78.13	27.67
C-276	20	-20938	3.626×10^{-11}	9.954×10^{5}	1.224×10^{-7}	-	1.490×10^{6}
TA2	20	4.548	7.423×10^{-4}	7.741	0.107	-	10.27

4. Conclusion

This study evaluates the corrosion resistance of four materials—S30408 stainless steel, S31603 stainless steel, C-276 alloy, and TA2 titanium alloy—exposed to various chloride-containing corrosive environments. The results show that S30408 stainless steel exhibited the lowest corrosion resistance, followed by S31603 stainless steel, while C-276 alloy and TA2 titanium alloy demonstrated superior performance. As the concentrations of chloride ions and hydrochloric acid increased, the corrosion resistance of all materials decreased. However, both TA2 titanium alloy and C-276 alloy maintained excellent performance even in highly concentrated corrosive environments.

(1) Full immersion tests demonstrated that TA2 and C-276 exhibit optimal corrosion resistance in organic chlorides, with corrosion rates ranked as S30408 > S31603 > C-276 > TA2.

(2) Electrochemical tests revealed that increased hydrochloric acid concentration (Cl^- enrichment) significantly accelerates material degradation: self-corrosion current density increases, while impedance radius and charge

transfer resistance decrease. The corrosion resistance hierarchy follows TA2 > C-276 > S31603 > S30408.

(3) S30408 and S31603 stainless steel in the service conditions there is a risk of sensitization, in the process should also be considered to control the Cl- concentration and water content, to sum up: it is recommended to use C-276 or TA2 material as the emergency cooling tower and heat exchanger equipment selection to ensure the safe operation of the equipment.

Acknowledgements

Special thanks to China National Institute of Special Equipment Testing and Research (CSEI) and Sinopec Hunan Chemical Co. for their help in the experimental equipment and testing in this study.

REFERENCES

[1] Penyaz M, Otto J L, Popov N, et al. Microstructure influence on corrosion resistance of brazed AISI 304L/NiCrSiB joints. Metals and Materials International, 2021, 27(10): 4142-4151. DOI: 10.1007/s12540-021-00974-z.

[2] Benea L, Bounegru I, Axente E R, et al. Susceptibility of 316L Stainless Steel Structures to Corrosion Degradation in Salivary Solutions in the Presence of Lactic Acid. Journal of Functional Biomaterials, 2023, 14(11): 535. DOI: 10.3390/jfb14110535.

[3] Zhai W, Zhou W and Nai SML. In-situ formation of TiC nanoparticles in selective laser melting of 316L with addition of micronsized TiC particles. Materials Science and Engineering a-Structural Materials Properties Microstructure and Processing 2022; 829. DOI: 10.1016/j.msea.2021.142179.

[4] Tanprayoon D, Srisawadi S, Sato Y, et al. Microstructure and hardness response of novel 316L stainless steel composite with TiN addition fabricated by SLM. Optics and Laser Technology 2020; 129. DOI: 10.1016/j.optlastec.2020.106238.

[5] Chen X, Fu Q, Gong M, et al. Influences of multi-factors on Corrosion Resistance of TA2 pure Titanium in Brine Solution Produced from Vacuum Salt Plant. International Journal of Electrochemical Science 2022; 17. DOI: 10.20964/2022.06.17.

[6] Guo C, Du X, He J, et al. Fabrication of submillimetre structures on pure titanium by non-aqueous electrolyte jet machining. International Journal of Advanced Manufacturing Technology 2024; 134: 4283-4295. DOI: 10.1007/s00170-024-14371-4.

[7] Zhang Y, Fan L, Liu Z, et al. Effect of Alternating Magnetic Field on Electrochemical Behavior of 316L and TA2 in Simulated Seawater. Journal of Materials Engineering and Performance 2021; 30: 9377-9389. DOI: 10.1007/s11665-021-06131-2.

[8] Yang X, Du C, Wan H, et al. Influence of sulfides on the passivation behavior of titanium alloy TA2 in simulated seawater environments. Applied Surface Science 2018; 458: 198-209. DOI: 10.1016/j.apsusc.2018.07.068.

[9] Ubaldini A, Telloli C, Rizzo A, et al. A Study of Accelerated Corrosion of Stainless Steels under Highly Oxidizing Conditions. Coatings, 2024, 14(4): 390. DOI: 10.3390/coatings14040390.

[10] Harsimran S, Santosh K, Rakesh K. Overview of corrosion and its control: A critical review. Proc. Eng. Sci, 2021, 3(1): 13-24. DOI: 10.24874/PES03.01.002.

[11] Sainis S, Persson D, Törne K, et al. The influence of recycling on the localized corrosion susceptibility of extruded AA6063 alloys. npj Materials Degradation, 2024, 8(1): 95. DOI:

10.1038/s41529-024-00510-5.
[12] Wang R, Huang Y, Jiang T, et al. Microstructure and Mechanical Properties of Niobium and 316L Stainless Steel Joints by TU1 Oxygen Free Copper Brazing. Rare Metal Materials and Engineering 2021; 50: 1166-1172.
[13] Liu Y, Guo J, Shi W, et al. Mechanical Properties of 316LStainless Steel Porous Structure Formed byLaser Powder Bed Fusion. Chinese Journal of Lasers, 2022; 49(08): 195-205.
[14] Vogiatzis C A, Kountouras D T, Skolianos S M. Corrosion behaviour of 304 stainless steel in simulated oilfield produced water. Corrosion Engineering, Science and Technology, 2016, 51(1): 51-59. DOI: 10.1179/1743278215Y.0000000033.
[15] Asgari M, Aliofkhazraei M, Olum A R, et al. Electrochemical behavior of 316 L stainless steel in alkaline environments containing chloride ion. Protection of Metals and Physical Chemistry of Surfaces, 2018, 54: 325-332. DOI: 10.1134/S2070205118020132.
[16] Jalali M, Najafisayar P. A Comparison of Localized Corrosion Behavior of Hastelloy X and Stainless Steel 316 in Persian Gulf Costal Water. Protection of Metals and Physical Chemistry of Surfaces, 2024, 60(3): 482-492. DOI: 10.1134/S2070205124701752.
[17] Zakerin N, Morshed-Behbahani K. Perspective on the passivity of Ti6Al4V alloy in H2SO4 and NaOH solutions. Journal of Molecular Liquids, 2021, 333: 115947. DOI: 10.1016/j.molliq.2021.115947.
[18] Wang D, Zhang J. Experimental research on the counter-rotating electrochemical machining of 304 stainless steel and Inconel 718 alloy. International Journal of Electrochemical Science, 2019, 14(10): 9741-9754. DOI: 10.20964/2019.10.26.
[19] Li L F, Daerden M, Caenen P, et al. Electrochemical behavior of hot-rolled 304 stainless steel during chemical pickling in HCl-based electrolytes. Journal of the Electrochemical Society 2006; 153: B145-B150. DOI: 10.1149/1.2177136.
[20] Öteyaka M Ö, Arslan A E, Çakir F H. Wear and corrosion characterisation of AISI 1030, AISI 1040 and AISI 1050 steel coated with Shielded Metal Arc Welding (SMAW) and Plasma Transfer Arc (PTA) methods. Sādhanā, 2021, 46(3): 134. DOI: 10.1007/s12046-021-01661-w.
[21] Geambazu L E, Cotruţ C M, Miculescu F, et al. Mechanically alloyed CoCrFeNiMo0. 85 high-entropy alloy for corrosion resistance coatings. Materials, 2021, 14(14): 3802. DOI: 10.3390/ma14143802.